Yuan, Shibo; Bai, Peng; He, Yi; Chen, Jiafa; Zhao, Yicheng; Li, Yongdan

Black TiO_2-supported copper nanoparticles for efficient photocatalytic N-formylation of N-methylaniline with CO_2

Published in:
Journal of CO2 Utilization

DOI:
10.1016/j.jcou.2023.102453

Published: 01/05/2023

Document Version
Publisher's PDF, also known as Version of record

Please cite the original version:
Yuan, S., Bai, P., He, Y., Chen, J., Zhao, Y., & Li, Y. (2023). Black TiO_2-supported copper nanoparticles for efficient photocatalytic N-formylation of N-methylaniline with CO_2. *Journal of CO2 Utilization*, *71*, Article 102453. https://doi.org/10.1016/j.jcou.2023.102453

Journal of CO2 Utilization 71 (2023) 102453

Contents lists available at ScienceDirect

Journal of CO2 Utilization

journal homepage: www.elsevier.com/locate/jcou

Black TiO_2-supported copper nanoparticles for efficient photocatalytic N-formylation of *N*-methylaniline with CO_2

Shibo Yuan [a,b,1], Peng Bai [a,b,1], Yi He [a,b], Jiafa Chen [a,b], Yicheng Zhao [a,b,*], Yongdan Li [a,b,c]

[a] *State Key Laboratory of Chemical Engineering (Tianjin University), Tianjin Key Laboratory of Applied Catalysis Science and Technology, School of Chemical Engineering and Technology, Tianjin University, Tianjin 300072, China*
[b] *Collaborative Innovation Center of Chemical Science and Engineering (Tianjin), Tianjin 300072, China*
[c] *Department of Chemical and Metallurgical Engineering, Aalto University, Kemistintie 1, FI-00076 Aalto, Finland*

ARTICLE INFO

Keywords:
Photocatalysis
N-formylation
CO_2 reduction
Black titanium dioxide
N-methylaniline

ABSTRACT

Photocatalytic N-formylation of amines with CO_2 is a promising strategy to convert CO_2 into value-added chemicals sustainably. In this work, a black TiO_2-supported Cu photocatalyst is prepared through a solvothermal method for the N-formylation of N-methylaniline with $NaBH_4$ as the reducing agent. Cu nanoparticles and oxygen vacancies are formed on the surface of the photocatalyst after reduction with H_2, which decreases the band-gap energy and promotes the separation of photogenerated electrons and holes, thereby improving the photocatalytic activity remarkably. A 100 % conversion is achieved after 9 h radiation, and the yield of *N*-methylformanilide reaches 81 %. Both the amount of $NaBH_4$ and the pressure of CO_2 show important influences on the activity and selectivity of the photocatalytic process, and the carbon and hydrogen in the aldehyde group are from CO_2 and $NaBH_4$, respectively. The photocatalyst also shows promising cycling durability.

1. Introduction

Large-scale consumption of fossil fuels causes excessive CO_2 emission into the atmosphere, leading to climate change and environmental problems [1,2]. Therefore, it is essential to develop CO_2 capture and conversion technologies [3–5]. Due to its non-toxicity and high abundance, CO_2 is considered as an ideal C_1 feedstock to produce value-added chemicals [6–9]. The utilization of CO_2 in the functionalization of N-H bonds has attracted much attention in recent years [10]. The synthesis of formamide and methylamine is important in the production of pharmaceuticals, agricultural chemicals, dyes, perfumes and key intermediates [11–14]. Using CO_2 and $PhSiH_3$ as the reactants, Cantat and coworkers [11,12] realized the formylation and methylation of amines with triaza bicyclodecene and zinc complexes as the catalysts, respectively, and high yields of 99 %–100 % are achieved after 20–24 h reaction at 100 °C. Liu et al. [15] synthesized N-doped carbon-supported Pd catalysts for the N-formylation of amines with CO_2 and H_2 at 130 °C. Lin et al. [16] developed a PdZn-TiO_2 catalyst and realized the *N*-methylation of *N*-methylaniline (MA) with a selectivity of 99.9 % using CO_2 and H_2 as the reductants at 180 °C. However, those thermocatalytic processes usually require external energy supply, high pressure and expensive noble metal or homogeneous catalysts. Recently, the N-formylation of amines with CO_2 is realized at room temperature using ionic liquids as the catalyst and $PhSiH_3$ as the reducing agent. [17,18] Photocatalytic formylation and methylation of amines with CO_2 under a moderate condition is a promising sustainable strategy. In 2021, Prajapati et al. [19] developed a CuO-$BiVO_4$ photocatalyst for the N-formylation of aniline with CO_2 using $PhSiH_3$ as the reducing agent, and a conversion of 85 % is reached after 24 h radiation. Using zinc phthalocyanine-C_3N_4 hybrid photocatalyst, Malik et al. [20] obtained a yield of 95 % for the N-formylation of morpholine. However, the mechanisms of those photocatalytic processes require further investigation, and the high cost of $PhSiH_3$ limits their practical application.

TiO_2 is one of the most commonly used semiconductor photocatalysts due to its abundance, low cost, non-toxicity and long-term stability [21–23]. However, the photocatalytic efficiency of TiO_2 is not satisfactory mainly because of the poor light absorption and severe charge carrier recombination [24–26]. In 2011, Chen et al. [27] prepared black TiO_2 photocatalyst via heat treatment in a high-pressure hydrogen atmosphere. The hydrogenation introduces disordered

---

* Corresponding author at: State Key Laboratory of Chemical Engineering (Tianjin University), Tianjin Key Laboratory of Applied Catalysis Science and Technology, School of Chemical Engineering and Technology, Tianjin University, Tianjin 300072, China.

E-mail address: zhaoyicheng@tju.edu.cn (Y. Zhao).

[1] These authors contributed equally to this work

https://doi.org/10.1016/j.jcou.2023.102453
Received 3 January 2023; Received in revised form 1 March 2023; Accepted 7 March 2023

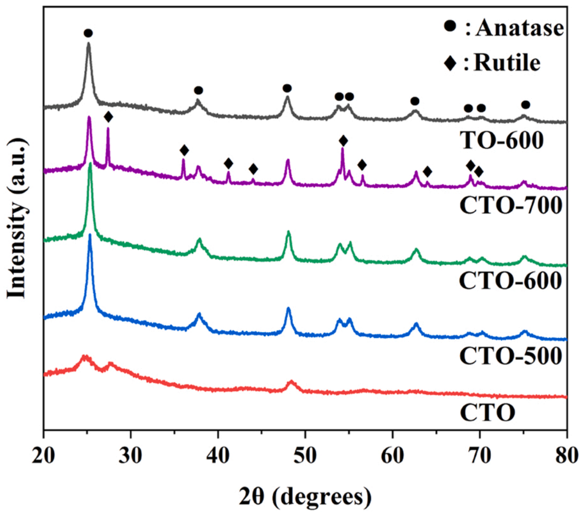

Fig. 1. XRD patterns of the samples.

surface layers, which enhance solar absorption and facilitate photoexcited electron-hole separation. In recent years, black TiO_2 has been widely studied in photocatalytic systems such as water splitting, organic pollutant removal and CO_2 reduction [28–30]. The abundant oxygen vacancy (O_V) in black TiO_2 is generally considered to be the main reason for the enhancement of photocatalytic activity.

The incorporation of cocatalysts is an effective strategy to improve the photocatalytic performance of black TiO_2. Noble metals such as Pt, Ru and Pd are commonly used to narrow the band gap, prevent the recombination of charge carriers and enhance the apparent quantum efficiency of black TiO_2 [31–34]. In addition, earth-abundant transition metals such as Fe and Ni are also alternatives as cocatalysts [35,36]. In 2016, Zhao et al. [37] prepared black TiO_2-coated Cu nanoparticles for CO_2 photoreduction. The metallic Cu enhances the absorption of visible light and promotes the separation of photoinduced electron-hole pairs. Choi et al. [38] incorporated Cu into g-C_3N_4/black TiO_2 nanofiber heterostructure for photocatalytic H_2 evolution and pollutant removal. Chen et al. [39] designed black TiO_2-Cu-ZnO Z-scheme heterojunction for photocatalytic water splitting. The ZnO nanolayer prepared by the atomic layer deposition technique protects the metallic Cu from oxidation.

Herein, we synthesize a Cu-black TiO_2 photocatalyst, which has demonstrated high promise to utilize solar energy efficiently, through a

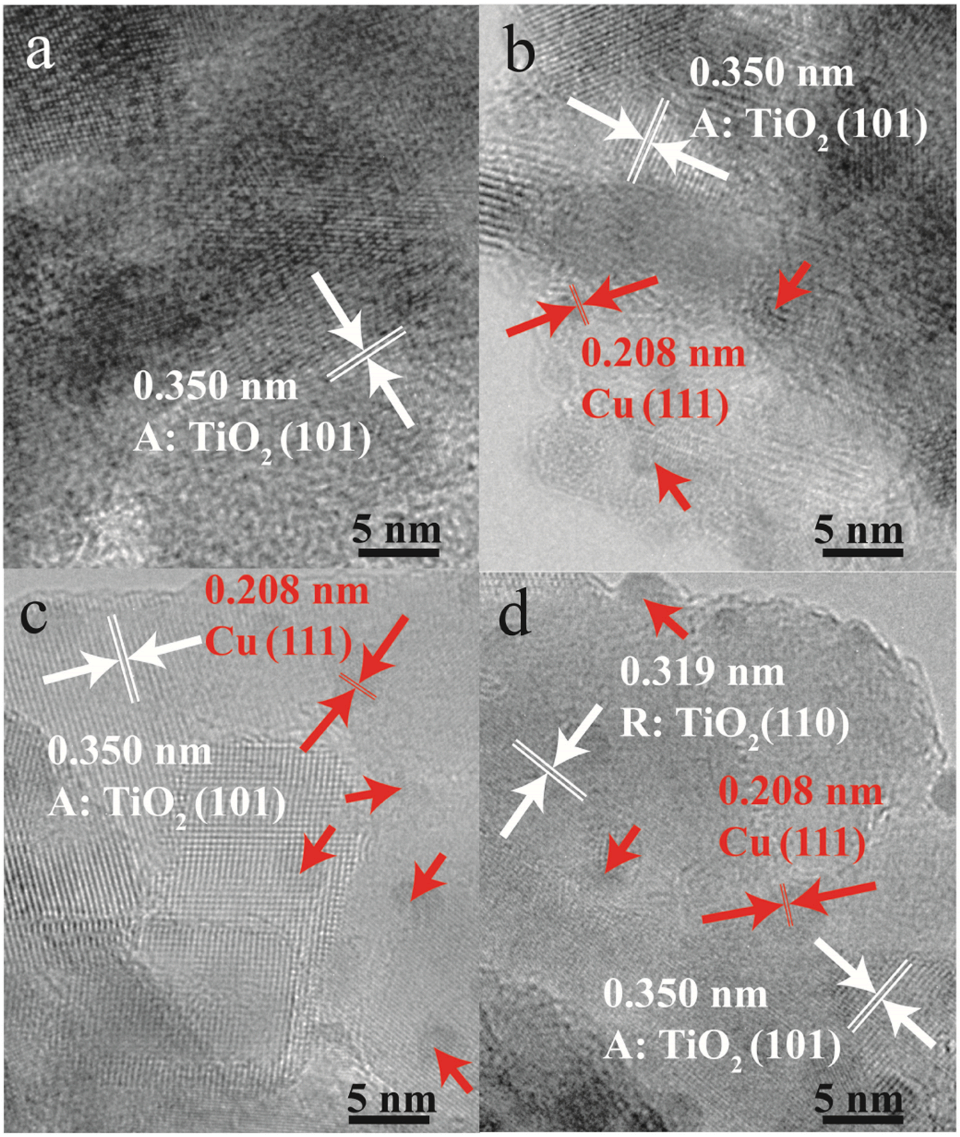

Fig. 2. TEM images of (a) TO-600, (b) CTO-500, (c) CTO-600 and (d) CTO-700. The red arrows indicate Cu nanoparticles.

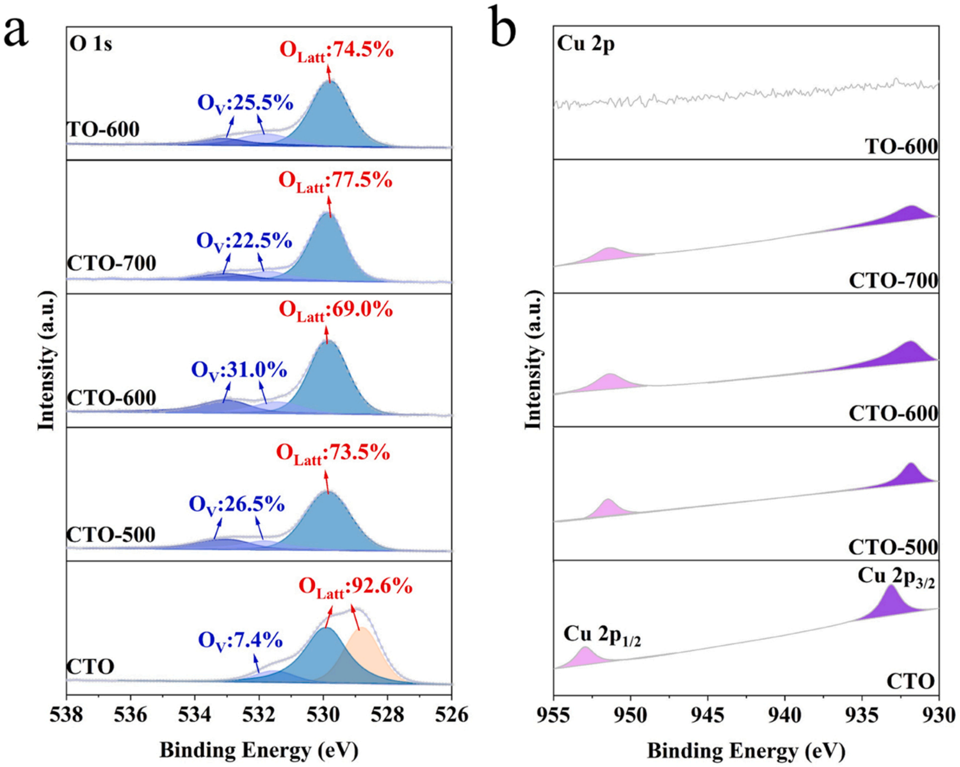

Fig. 3. High-resolution XPS of (a) O 1 s and (b) Cu 2p of the photocatalysts.

solvothermal process for the N-formylation of MA with CO_2. Cost-effective $NaBH_4$ is used as the reducing agent. The composite catalyst exhibits promising activity and stability. Meanwhile, a possible mechanism of the photocatalytic process is proposed.

2. Experimental

2.1. Materials

Titanium tetrachloride ($TiCl_4$, 99.0 %) and copper nitrate hydrate ($Cu(NO_3)_2{\cdot}3H_2O$, 99 %) were from Shanghai Macleans Biochemical Technology Co., Ltd. Absolute ethanol (C_2H_5OH, AR) was purchased from Tianjin Jiangtian Chemical Technology Co., Ltd. MA was obtained from Shanghai Aladdin Biochemical Technology Co., Ltd. Ethylene glycol ($(CH_2OH)_2$, AR) and acetonitrile (CH_3CN, HPLC) were from Tianjin Komiou Chemical Reagent Co., Ltd. Sodium borohydride ($NaBH_4$, 98 %) was purchased from Shanghai Titan Technology Co., Ltd.

2.2. Catalyst preparation

1 wt. % Cu-TiO_2 (CTO) catalyst was synthesized through a facile solvothermal method [40]. Specifically, 1 mL $TiCl_4$ was dropwise added into 30 mL $(CH_2OH)_2$ and stirred at room temperature until the yellow complex was completely dissolved. Then, 1 mL of deionized water and stoichiometric $Cu(NO_3)_2{\cdot}3H_2O$ were added into the solution under continuous stirring. The obtained mixture was further stirred for 30 min and then transferred into a 150 mL Teflon-lined stainless-steel autoclave, followed by heating at 150 °C for 8 h. After cooling to room temperature, the white precipitate was washed with deionized water and ethanol for three times, respectively, and dried at 60 °C overnight. Finally, the powder was reduced with H_2 for 5 h at 500, 600 and 700 °C, and the obtained catalysts were marked as CTO-500, CTO-600 and CTO-700, respectively. For comparison, bare TiO_2 (TO) was prepared without the addition of $Cu(NO_3)_2{\cdot}3H_2O$ following the same procedure, and 1 wt. % Pt-TiO_2 (PtTO) and 1 wt. % Pd-TiO_2 (PdTO) were also synthesized with the addition of stoichiometric H_2PtCl_6 and $PdCl_2$.

2.3. Characterization

The crystal structures of the catalysts were determined by X-ray diffraction (XRD) using a D8-focused diffractometer (Bruker Corp., Germany) with a Cu-Kα radiation source (λ = 1.54056 Å). The morphology and microstructure of the samples were observed with a scanning electron microscope (SEM, S-4800, Hitachi, Japan) and a transmission electron microscope (TEM, JEM-2100 F, JEOL Inc., Japan). The N_2 adsorption isotherms of the samples were measured using a BELSORP-mini analyzer (MicrotracBEL, Japan), and the specific surface areas of the photocatalysts were determined with the Brunauer-Emmett-Teller (BET) equation. The surface chemical state of the samples was analyzed with an ESCALAB 250 Xi X-ray photoelectron spectrometer (XPS, Thermo-VG Scientific, USA) using Al-Kα ($h\nu = 1486.6$ eV) as the X-ray source, and the binding energies were calibrated against the C 1 s peak at 284.8 eV. The ultra-violet-visible (UV–vis) absorption spectra were measured with a Hitachi-3900 UV–vis spectrophotometer in the range of 200–800 nm, and $BaSO_4$ was selected as a reference. Photoluminescence spectra (PL) of the samples were recorded using a Fluorolog-3 spectrometer (HORIBA Jobin Yvon, USA) with a 380 nm excitation wavelength.

The photoelectrochemical properties of the samples were tested using a CHI-660B electrochemical workstation (CH Instruments, USA) with a three-electrode system in a quartz glass electrolytic cell. The working electrode was prepared by dispersing 2 mg of the photocatalyst powder into 25 μL ethanol and 10 μL Nafion under ultrasonication, which was then coated onto a 1.0×2.0 cm^2 fluorine-doped tin oxide (FTO) glass and dried at 60 °C. Pt was used as the counter electrode and Ag/AgCl was used as the reference electrode. The photocurrent response, the electrochemical impedance spectroscopy (EIS) and the Mott-Schottky plot tests were carried out in a 0.5 mol L^{-1} Na_2SO_4 aqueous solution. The frequency range of the EIS measurement was from 100 kHz to 0.1 Hz. The test frequencies of the Mott-Schottky plots were

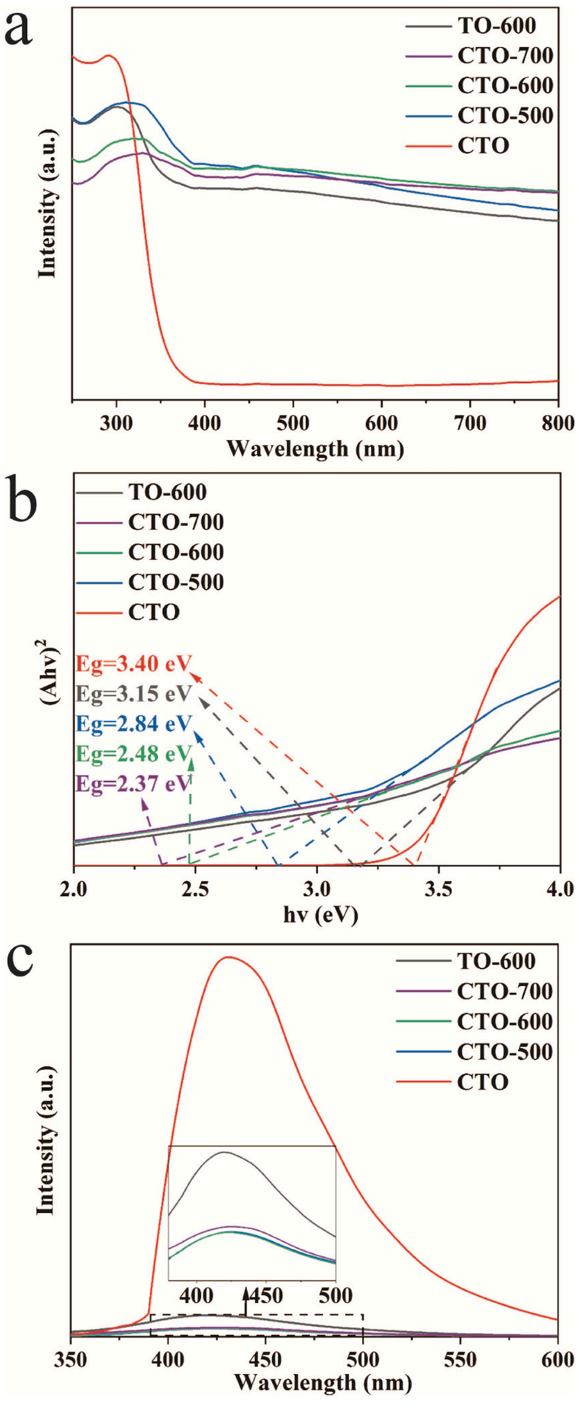

Fig. 4. (a) UV–vis absorption, (b) band-gap energy and (c) PL spectra of the samples.

800, 1000 and 1200 Hz.

2.4. Photocatalytic reaction

In a typical reaction, 10 mg of photocatalyst, 50 mg of MA, 5 mL of CH_3CN (ACN) and 50 mg of $NaBH_4$ were added into a 50 mL autoclave reactor equipped with a glass window. The photocatalytic test was performed with magnetic stirring under 0.5 MPa of CO_2. Light irradiation was provided by a CEL-HXF300 Xe lamp (CEAuLight, China). The liquid products were qualitatively analyzed with a gas chromatograph-mass spectrometer (GC-MS, GC-Agilent 6890 A and MS-Agilent 5973 C) and then quantitatively analyzed using gas chromatography (GC, Shimadzu, Japan) with a flame ionization detector and an SH-Rtx-1 capillary column (30 m × 0.25 mm×0.25 μm). The liquid products were also characterized with ^1H and ^{13}C nuclear magnetic resonance (NMR) using a Bruker spectrometer (AVANCE III HD 400). The gaseous product was analyzed using a GC (Shimadzu GC-2014 C) with a thermal conductivity detector and a TDX-101 packed column.

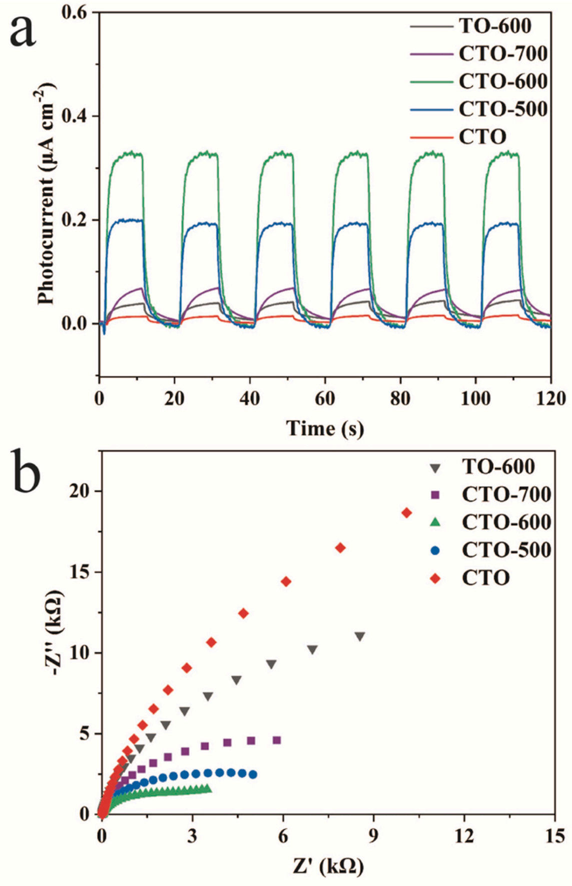

Fig. 5. (a) Photocurrent responses and (b) EIS curves of the samples.

3. Results and discussion

3.1. Characterization

The TO and CTO powders before reduction both exhibit a white colour, which changes to black after reduction, indicating the formation of black TiO_2 (Fig. S1). The XRD pattern of CTO without reduction shows mixed anatase (JCPDS 21–1272) and rutile (JCPDS 21–1276) structures with a low degree of crystallinity (Fig. 1). After the reduction at 500 or 600 °C, the anatase phase becomes more crystalline, while the rutile phase disappears. However, when the reduction temperature increases to 700 °C, the mixed anatase-rutile structure forms again. The structure of bare TiO_2 reduced at 600 °C is similar to that of CTO-600. The SEM image of CTO shows a flower-like morphology composed of nanowires (Fig. S2) with a BET surface area of 219.1 $m^2\ g^{-1}$ (Table S1). Agglomeration is observed with the rise of the reduction temperature, and the surface area decreases to 60–80 $m^2\ g^{-1}$ accordingly.

Fig. 2 shows the TEM images of the samples. Lattice fringes with a spacing of 0.350 nm corresponding to the (101) crystal plane of anatase TiO_2 are observed in TO-600 (Fig. 2a) [41]. With the addition of Cu, particles with an average size of about 5 nm are found, and the interplanar spacing of 0.208 nm can be attributed to the Cu (111) facet (Fig. 2b-d) [42,43]. Besides, the (110) plane of rutile TiO_2 with a spacing of 0.319 nm is also observed in CTO-700 (Fig. 2d), which is consistent

Table 1

N-formylation reaction of *N*-methylaniline with CO_2 under various conditions.

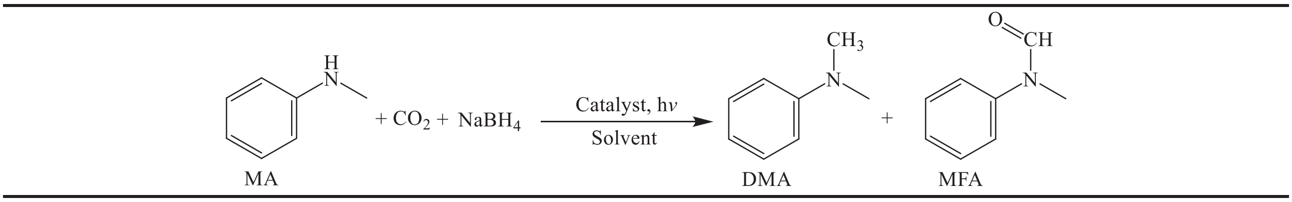

Entry	Catalyst		Reaction Time (h)	Solvent	Conversion (%)	Yields (%)	
	Reducing temperature (°C)	Cu loading (wt. %)				DMA	MFA
1	no catalyst		3	ACN	22.5	14.0	8.5
2	no reduction	1	3	ACN	26.2	15.0	11.2
3	500	1	3	ACN	62.6	22.5	40.1
4	600	1	3	ACN	69.9	18.1	51.8
5	700	1	3	ACN	58.6	22.5	36.1
6	600	0	3	ACN	54.0	23.6	30.4
7	600	0.5	3	ACN	62.9	21.4	41.5
8	600	2	3	ACN	62.8	22.0	40.8
9	600	3	3	ACN	53.2	22.8	30.4
10	600	1	0.5	ACN	20.9	13.8	7.1
11	600	1	1	ACN	38.6	17.0	21.6
12	600	1	6	ACN	90.9	18.7	72.2
13	600	1	9	ACN	100	19.0	81.0
14	600	1	9	DCM	0	0	0
15	600	1	9	THF	33.5	17.8	14.7
16	600	1	9	DMF	16.1	4.3	11.8
17	600	1	9	DMSO	5.9	2.9	3.0

Reaction condition: 50 mg of substrate, 10 mg of catalyst, 50 mg of $NaBH_4$, in 5 mL of solvent, under 0.5 MPa of CO_2, 25 °C, under Xe lamp irradiation.

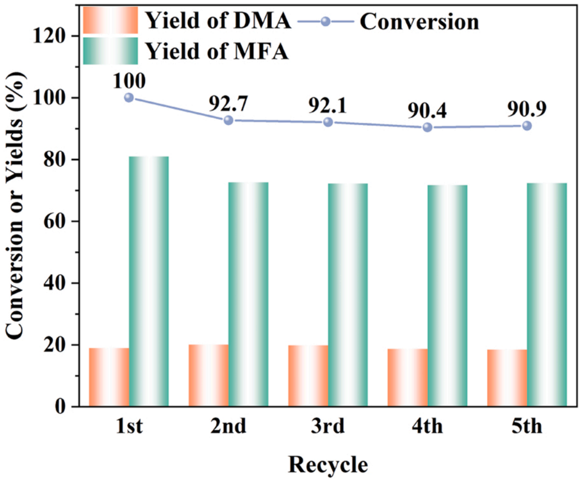

Fig. 6. Stability of CTO-600 catalyst during five 9-hour reaction cycles.

with the XRD results (Fig. 1).

The O 1 s XPS curve of CTO can be resolved into three peaks (Fig. 3a). The two peaks at 528.8 and 529.9 eV are assigned to lattice oxygen (O_{Latt}) in TiO_2 [27], and the other peak at 531.6 eV is attributed to oxygen species adsorbed on surface O_V [37]. The peak at 528.8 eV disappears after reduction. Meanwhile, another peak at about 533.1 eV is observed, which can be ascribed to oxygen in surface hydroxyl groups adsorbed on O_V [44]. The rise of the reduction temperature results in more O_V. Nevertheless, the O_V content of CTO-700 is lower than that of CTO-600 probably due to the formation of the rutile phase. Furthermore, the O_V concentration of CTO-600 is higher than that of TO-600, indicating that Cu species facilitate the reduction of TiO_2.

The Cu 2p XPS curves of the samples are shown in Fig. 3b. The peaks at 953.1 and 933.2 eV in the result of CTO can be ascribed to Cu^{2+}, which move to lower binding energies (951.7 and 931.6 eV) corresponding to Cu^+ or Cu^0 after reduction [45,46]. Though it is difficult to distinguish between Cu^+ and Cu^0 in the XPS results, the Cu LMM Auger spectra involving Cu^0 peaks at 565.2 eV but no Cu^+ peaks at 571.1 eV indicate that Cu^{2+} is reduced to Cu^0 rather than Cu^+ (Fig. S3) [47,48].

3.2. Photochemical properties

Fig. 4a shows the UV–vis absorption spectra of the samples. The absorption edge of CTO is about 380 nm, and its band-gap energy (*Eg*) calculated based on the Tauc plot is 3.40 eV (Fig. 4b). The light absorption region is broadened with the rise of reduction temperature probably attributed to the formation of more O_V for CTO-500 and CTO-600 and the rutile phase for CTO-700, and the *Eg* of CTO-500, CTO-600 and CTO-700 are 2.84, 2.48 and 2.37 eV, respectively. Meanwhile, the *Eg* of CTO-600 is much lower than that of TO-600 (3.15 eV), demonstrating that Cu promotes light absorption of the TiO_2 catalyst after reduction. Fig. 4c shows the PL spectra of the samples. CTO shows a high emission intensity due to severe charge carrier recombination [49]. The luminescence intensity decreases significantly after reduction, demonstrating the enhancement of separation efficiency of photoinduced electron-hole pairs. The intensity of CTO-600 is much lower than that of TO-600, which could be explained by the effective promotion of photogenerated electron extraction to Cu active sites and the more Ov [50, 51].

The photoelectrochemical activities of the samples are studied with photocurrent response and EIS measurements. CTO exhibits the lowest photocurrent density (Fig. 5a) and the highest charge transfer resistance (the arc in Fig. 5b). The photocurrent of CTO-500 is higher than that of CTO due to the improved light absorption ability (Fig. 4a) as well as the enhanced electron-hole separation efficiency (Fig. 4c), corresponding to a lower charge transfer resistance. CTO-600 obtains the highest current density and the lowest resistance, suggesting the best photoactivity. CTO-700 with a mixed anatase-rutile structure shows a lower activity compared with CTO-600. Besides, the photoelectrochemical activity of CTO-600 is much higher than that of TO-600.

Table 2
The substrate scope of *N*-methylation and N-formylation.

Entry	Substrate	Products		Conversion (%)	Yields (%)	
	1	**2**	**3**		**2**	**3**
1	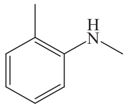	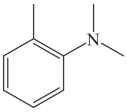	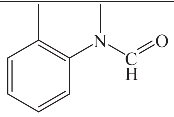	100	19.1	80.9
2	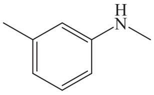	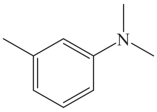	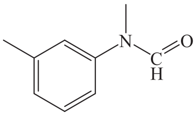	100	19.7	80.3
3	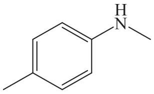	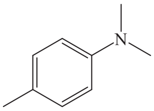	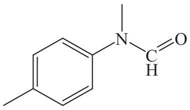	100	18.8	81.2
4	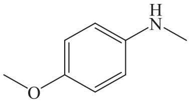	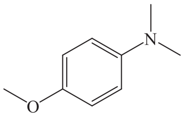	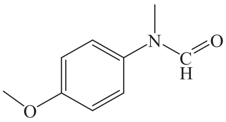	100	16.6	83.4
5	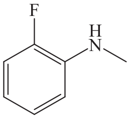	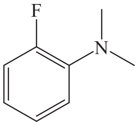	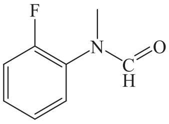	70.4	48.4	22.0
6	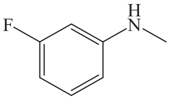	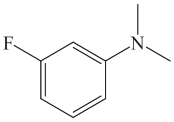	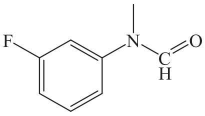	78.3	47.4	30.9
7	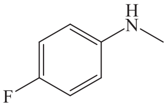	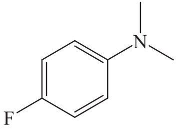	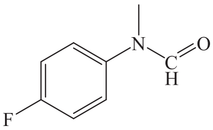	100	29.1	70.9
8	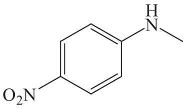	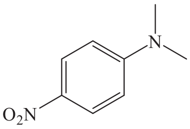	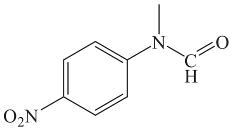	0	0	0

Reaction condition: 50 mg of substrate, 10 mg of catalyst, 50 mg of $NaBH_4$, in 5 mL of ACN, under 0.5 MPa of CO_2, 25 °C, 9 h, under Xe lamp irradiation.

3.3. Photocatalytic performance

The products of the photocatalytic reaction between MA and CO_2 with $NaBH_4$ as the reducing agent are mainly N, N-dimethylaniline (DMA) and *N*-methylformanilide (MFA) (Figs. S4 and S5). As shown in Table 1, A small amount (22.5 %) MA is converted after 3 h irradiation under a CO_2 partial pressure (P_{CO2}) of 0.5 MPa without any catalyst (entry 1). With CTO as the photocatalyst, the conversion of MA is 26.2 % and the yields of MFA and DMA are 11.2 % and 15.0 %, respectively (entry 2). The conversions with the reduced catalysts are much higher than that over the CTO catalyst (entries 3–5). The highest conversion of 69.9 % is reached using CTO-600 as the catalyst with 51.8 % and 18.1 % yields of MFA and DMA, respectively (entry 4). The performances of the photocatalysts with various Cu loading amounts are also studied (entries 4, 6–9), and the catalyst with 1 wt. % Cu shows the highest activity. The complete conversion of MA is achieved after 9-hour reaction with CTO-600 catalyst, during which period the yield of MFA increases gradually, while that of DMA reaches an almost constant value in the first hour (entries 4, 10–13). Furthermore, the solvent shows significant effects on the conversion of MA and the yields of the products (entries 14–17). The

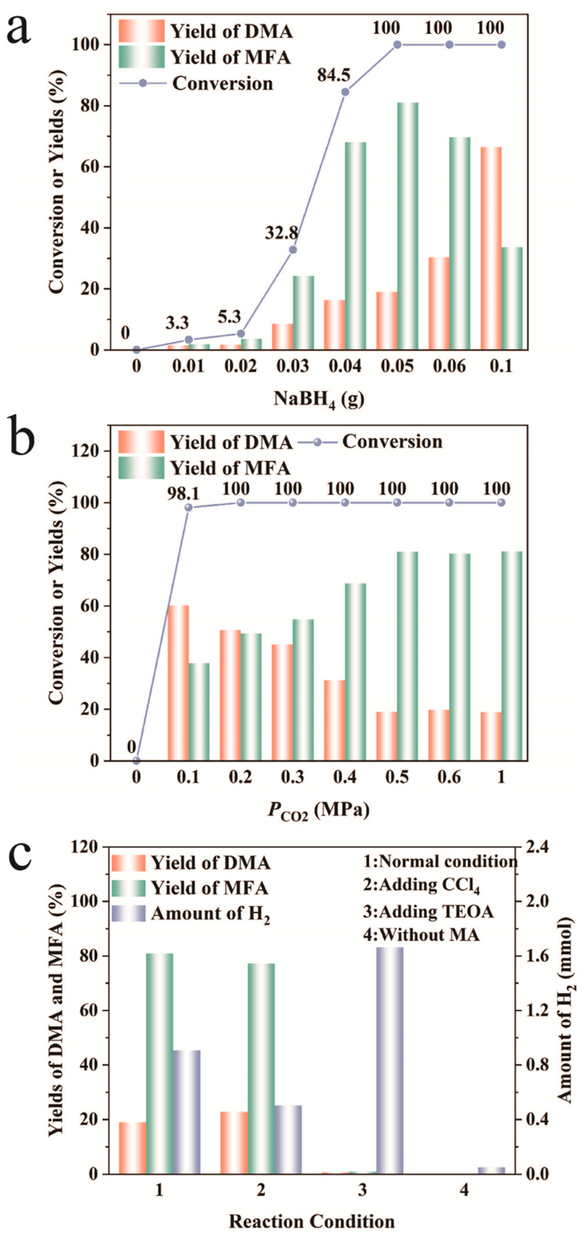

Fig. 7. The conversion of MA and the yields of the products after 9 h reaction over CTO-600 with various (a) $NaBH_4$ amounts and (b) P_{CO2}. (c) The performance of CTO-600 photocatalyst under various reaction conditions.

conversion is reduced remarkably when ACN is replaced by other common organic solvents such as dichloromethane (DCM), tetrahydrofuran (THF), dimethylformamide (DMF) and dimethyl sulfoxide (DMSO).

For comparison, we prepared Cu-based photocatalyst with commercial P25 TiO_2, and reduced it with H_2 at 600 ℃ for 5 h (marked as P25–600). The activity and selectivity of P25–600 (Table S2, entry 1) are lower than those of TO-600 synthesized in this work (Table 1, entry 6). We also replaced Cu in CTO-600 with Pt and Pd, and the photocatalysts are named as PtTO-600 and PdTO-600, respectively. The activity and selectivity of PtTO-600 and PdTO-600 (Table S2, entries 2–3) are both lower than those of CTO-600 (Table 1, entry 4). Besides, CTO-600 shows relatively stable activity in five 9-hour photocatalytic reaction cycles (Fig. 6) without obvious change in the crystal structure and surface chemical properties (Figs. S6 and S7), demonstrating the good durability of the catalyst.

The scope of the reaction was evaluated with various substituents on the aromatic ring of *N*-methylaniline. As shown in Table 2, the conversion and selectivity of the N-formylation reaction after 9 h radiation change negligibly when methyl, as a weak electron-donating substituent, is added on the phenyl ring (entries 1–3). The selectivity of the N-formylation reaction is improved slightly when methyl is replaced by methoxyl with a stronger electron-donating ability (entry 4). On the contrary, the activity and selectivity of the N-formylation reaction both decrease with an electron-withdrawing fluorine substituent on the aromatic ring (entries 5–7) probably due to the nucleophilicity of the reaction, and the conversion and selectivity show an order of ortho- < meta- < para-substitution. The reaction is stopped with nitryl as a strong electron-withdrawing substituent (entry 8).

3.4. Reaction mechanism

The effects of $NaBH_4$ and CO_2 on photocatalytic activity are investigated. As shown in Fig. 7a, no products are generated without $NaBH_4$. The yields of DMA and MFA both increase with the addition of $NaBH_4$ until a 100 % conversion of MA is achieved when the amount of $NaBH_4$ reaches 0.05 g. The further addition of $NaBH_4$ results in more DMA and less MFA. The reaction stops when there is no CO_2 in the system (Fig. 7b), while an almost complete conversion is obtained under 0.1 MPa of CO_2. The yields of MFA and DMA increase and decrease, respectively, with the rise of P_{CO2} from 0.1 to 0.5 MPa, and keep constant when P_{CO2} is further increased.

To elucidate the mechanism of the reaction further, isotope-labeled $^{13}CO_2$ and $NaBD_4$ are used as feedstocks. The GC-MS results (Figs. S8 and S9) demonstrate that in the newly formed methyl group of DMA and the aldehyde group of MFA, the carbon and hydrogen atoms are from CO_2 and $NaBH_4$, respectively. The gas product of the reaction is mainly H_2, and the yields of DMA and MFA and the generation rate of hydrogen with $NaBD_4$ as the reducing agent under various reaction conditions are shown in Fig. 7c. 0.909 mmol hydrogen is produced under normal conditions after 9 h reaction, which mainly consists of HD (Fig. S10), indicating that hydrogen product derives from the reaction between MA and $NaBD_4$. With the addition of CCl_4 as an electron scavenger, the yields of DMA and MFA change negligibly, while the generation rate of hydrogen is suppressed remarkably, which suggests the importance of photoinduced electrons in the formation of hydrogen. On the other hand, when triethanolamine (TEOA) is added to the system as a sacrifice agent of holes, the conversion of MA almost stops, demonstrating that the oxidation of MA by photogenerated holes is a key step. Nevertheless, the production of hydrogen is significantly promoted probably due to the facilitated formation of electrons. Only a tiny amount of hydrogen is formed without MA in the system.

Based on the results above, a possible photocatalytic reaction mechanism is proposed (Scheme 1) [52–55]. Compared with the catalyst without reduction, the catalysts after reduction have more O_V (Fig. 3a), resulting in a narrower band gap and the enhancement of the light absorption capacity (Figs. 4a and 4b). The results of the Mott-Schottky plot (Fig. S11) and the Tauc plot (Fig. 4b) indicate that the conduction and valence band levels of the CTO-600 catalyst with the highest activity are $-$ 0.39 and 2.09 eV, respectively. Meanwhile, O_V also acts as an electron trapper, which promotes the separation of photogenerated charge carriers and improves the efficiency (Fig. 4c). As shown in Scheme 1, electrons and holes are generated on the surface of the CTO-600 catalyst under light irradiation. MA is oxidized by holes, forming H^+ and radical I. At the same time, CO_2 reacts with $NaBH_4$ and generates intermediates II and III gradually [52]. Radical I can react with intermediates II and III, forming MFA and DMA, respectively [53]. Therefore, the increase of P_{CO2} will improve the selectivity of intermediate II and the yield of MFA (Fig. 7b), while more $NaBH_4$ results in a higher selectivity of intermediate III and an enhanced yield of DMA (Fig. 7a). Besides, H/H^+ derived from byproduct IV might react with H^+ from MA and photoinduced electrons to form H_2, which, however, is a complicated process and requires further in-depth study.

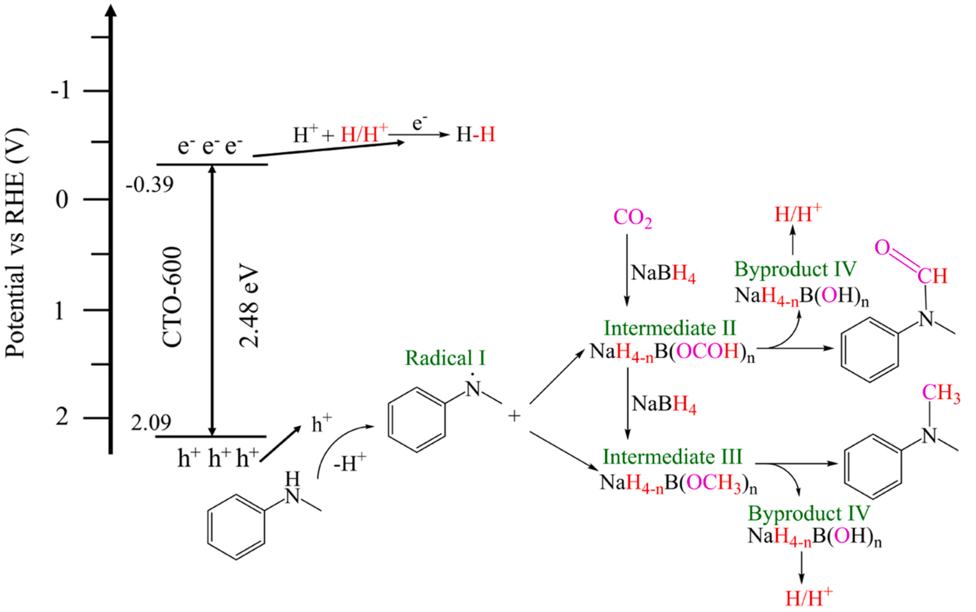

Scheme 1. A plausible mechanism of the photocatalytic reaction between MA and CO_2 with $NaBH_4$ as the reducing agent over CTO-600 catalyst.

4. Conclusion

In summary, a black TiO_2-supported Cu photocatalyst is developed for the N-formylation of MA to MFA with CO_2. TiO_2 shows an anatase structure after reduction at 600 °C, and more O_V are formed on the reduced samples. Cu nanoparticles with an average size of about 5 nm are observed on the surface of the reduced catalyst. The formation of O_V and Cu nanoparticles decreases the *Eg* of the photocatalyst and promotes the separation of photogenerated charge carriers, thus improving the photocatalytic efficiency significantly. CTO-600 shows the highest photocatalytic activity. A complete conversion of MA is achieved after 9 h radiation with $NaBH_4$ as the reducing agent, and the yields of MFA and DMA are 81.0 % and 19.0 %, respectively. The catalyst exhibits good cycling stability. Both the amount of $NaBH_4$ and P_{CO2} show important influences on the yield of MFA. The isotope-labeled results indicate that carbon and hydrogen in the aldehyde group are from CO_2 and $NaBH_4$, respectively. A possible mechanism of the photocatalytic process is proposed. This black TiO_2 with Cu nanoparticles is a promising photocatalyst for N-formylation of amines combined with high-efficiency CO_2 conversion.

CRediT authorship contribution statement

Shibo Yuan: Investigation, Validation, Writing – original draft, Visualization, **Peng Bai**: Conceptualization, Methodology, **Yi He**: Investigation, Validation, **Jiafa Chen**: Investigation, Validation, **Yicheng Zhao**: Resources, Supervision, Visualization, Writing – review & editing, Funding acquisition, **Yongdan Li**: Supervision, Project administration, Funding acquisition.

Declaration of Competing Interest

The authors declare that they have no known competing financial interests or personal relationships that could have appeared to influence the work reported in this paper.

Data Availability

Data will be made available on request.

Acknowledgments

This work was supported by the National Key Research and Development Program of China (2022YFB4101800). The financial support from the National Natural Science Foundation of China under contract number 22075205 is gratefully acknowledged. The work has been also supported by the Program of Introducing Talents to the University Disciplines under file number B06006, and the Program for Changjiang Scholars and Innovative Research Teams in Universities under file number IRT 0641.

Appendix A. Supporting information

Supplementary data associated with this article can be found in the online version at doi:10.1016/j.jcou.2023.102453.

References

[1] A. Mardani, D. Streimikiene, F. Cavallaro, N. Loganathan, M. Khoshnoudi, Sci. Total Environ. 649 (2019) 31–49.
[2] R.S. Haszeldine, S. Flude, G. Johnson, V. Scott, A. Mardani, D. Streimikiene, F. Cavallaro, N. Loganathan, M. Khoshnoudi, Philos. Trans. R. Soc. A Math. Phys. Eng. Sci. 376 (2018) 31–49.
[3] P.R. Yaashikaa, P. Senthil Kumar, S.J. Varjani, A. Saravanan, J. CO_2 Util. 33 (2019) 131–147.
[4] C. Hepburn, E. Adlen, J. Beddington, E.A. Carter, S. Fuss, N. Mac Dowell, J.C. Minx, P. Smith, C.K. Williams, Nature 575 (2019) 87–97.
[5] J. Wu, X.D. Zhou, Chin. J. Catal. 37 (2016) 999–1015.
[6] Q. Yi, T. Liu, X. Wang, Y. Shan, X. Li, M. Ding, L. Shi, H. Zeng, Y. Wu, Appl. Catal. B Environ. 283 (2021), 119620.
[7] Q. Liu, L. Wu, R. Jackstell, M. Beller, Nat. Commun. 6 (2015) 1–15.
[8] F.A. Rahman, M.M.A. Aziz, R. Saidur, W.A.W.A. Bakar, M.R. Hainin, R. Putrajaya, N.A. Hassan, Renew. Sustain. Energy Rev. 71 (2017) 112–126.
[9] C. Wu, Y. Zhou, Z. Zou, Chin. J. Catal. 32 (2011) 1565–1572.
[10] S. Lin, J. Liu, L. Ma, J. CO_2 Util. 54 (2021), 101759.
[11] A. Tlili, X. Frogneux, E. Blondiaux, T. Cantat, Angew. Chem. Int. Ed. 53 (2014) 2543–2545.
[12] C. Das Neves Gomes, O. Jacquet, C. Villiers, P. Thuéry, M. Ephritikhine, T. Cantat, Angew. Chem. Int. Ed. 51 (2012) 187–190.
[13] O. Jacquet, X. Frogneux, C. Das Neves Gomes, T. Cantat, Chem. Sci. 4 (2013) 2127–2131.
[14] K. Beydoun, G. Ghattas, K. Thenert, J. Klankermayer, W. Leitner, Angew. Chem. Int. Ed. 53 (2014) 11010–11014.
[15] X. Luo, H. Zhang, Z. Ke, C. Wu, S. Guo, Y. Wu, B. Yu, Z. Liu, Sci. China Chem. 61 (2018) 725–731.
[16] W. Lin, H. Cheng, Q. Wu, C. Zhang, M. Arai, F. Zhao, ACS Catal. 10 (2020) 3285–3296.

[17] X.Y. Li, H.C. Fu, X.F. Liu, S.H. Yang, K.H. Chen, L.N. He, Catal. Today 356 (2020) 563–569.
[18] A. Gopakumar, L. Lombardo, Z. Fei, S. Shyshkanov, D. Vasilyev, A. Chidambaram, K. Stylianou, A. Züttel, P.J. Dyson, J. CO_2 Util. 41 (2020), 101240.
[19] P.K. Prajapati, S. Saini, N. Nandal, S.L. Jain, J. CO_2 Util. 45 (2021), 101402.
[20] A. Malik, P.K. Prajapati, B.M. Abraham, S. Bhatt, P. Basyach, S.L. Jain, Catal. Sci. Technol. 12 (2022) 2688–2702.
[21] J. Wen, X. Li, W. Liu, Y. Fang, J. Xie, Y. Xu, Chin. J. Catal. 36 (2015) 2049–2070.
[22] Q. Guo, C. Zhou, Z. Ma, X. Yang, Adv. Mater. 31 (2019), 1901997.
[23] S.N. Habisreutinger, L. Schmidt-Mende, J.K. Stolarczyk, Angew. Chem. Int. Ed. 52 (2013) 7372–7408.
[24] M. Humayun, F. Raziq, A. Khan, W. Luo, Green. Chem. Lett. Rev. 11 (2018) 86–102.
[25] K. Qi, B. Cheng, J. Yu, W. Ho, Chin. J. Catal. 38 (2017) 1936–1955.
[26] T. Zhang, X. Han, N.T. Nguyen, L. Yang, X. Zhou, Chin. J. Catal. 43 (2022) 2500–2529.
[27] X. Chen, L. Liu, P.Y. Yu, S.S. Mao, Science 331 (2011) 746–750.
[28] J. Pan, Z. Dong, B. Wang, Z. Jiang, C. Zhao, J. Wang, C. Song, Y. Zheng, C. Li, Appl. Catal. B Environ. 242 (2019) 92–99.
[29] S. Wu, X. Li, Y. Tian, Y. Lin, Y.H. Hu, Chem. Eng. J. 406 (2021), 126747.
[30] R. Li, Q. Luan, C. Dong, W. Dong, W. Tang, G. Wang, Y. Lu, Appl. Catal. B Environ. 286 (2021), 119832.
[31] L. Zhang, L. Liu, Z. Pan, R. Zhang, Z. Gao, G. Wang, K. Huang, X. Mu, F. Bai, Y. Wang, W. Zhang, Z. Cui, L. Li, Nat. Energy 7 (2022) 1042–1051.
[32] B. Han, W. Wei, L. Chang, P. Cheng, Y.H. Hu, ACS Catal. 6 (2016) 494–497.
[33] C. Yuan, Y. Shen, C. Zhu, P. Zhu, F. Yang, J. Liu, C. An, ACS Sustain. Chem. Eng. 10 (2022) 10311–10317.
[34] Y. Xu, C. Zhang, L. Zhang, X. Zhang, H. Yao, J. Shi, Energy Environ. Sci. 9 (2016) 2410–2417.
[35] X. Wu, X. Wang, Y. Xie, N. Ren, J. Ma, P. Ning, Appl. Catal. B Environ. 310 (2022), 121325.
[36] T. Billo, F.Y. Fu, P. Raghunath, I. Shown, W.F. Chen, H.T. Lien, T.H. Shen, J.F. Lee, T.S. Chan, K.Y. Huang, C.I. Wu, M.C. Lin, J.S. Hwang, C.H. Lee, L.C. Chen, K. H. Chen, Small 14 (2018) 1–11.
[37] J. Zhao, Y. Li, Y. Zhu, Y. Wang, C. Wang, Appl. Catal. A Gen. 510 (2016) 34–41.
[38] J.U. Choi, Y.G. Kim, W.K. Jo, Appl. Surf. Sci. 473 (2019) 761–769.
[39] B. Chen, J. Zhang, J. Yu, R. wang, B. He, J. Jin, H. Wang, Y. Gong, J. Colloid Interface Sci. 607 (2022) 760–768.
[40] P. Bai, X. Tong, Y. Gao, P. Guo, Catal. Sci. Technol. 9 (2019) 5803–5811.
[41] J. Qu, Y. Wang, X. Mu, J. Hu, B. Zeng, Y. Lu, M. Sui, R. Li, C. Li, Adv. Mater. 34 (2022), 2203320.
[42] P.A. Desario, J.J. Pietron, T.H. Brintlinger, M. McEntee, J.F. Parker, O. Baturina, R. M. Stroud, D.R. Rolison, Nanoscale 9 (2017) 11720–11729.
[43] C. Li, Y. Yang, W. Ren, J. Wang, T. Zhu, W. Xu, Catal. Lett. 150 (2020) 2045–2055.
[44] J. Gao, Q. Shen, R. Guan, J. Xue, X. Liu, H. Jia, Q. Li, Y. Wu, J. CO_2 Util. 35 (2020) 205–215.
[45] X. Ma, J. Zhang, B. Wang, Q. Li, S. Chu, Appl. Surf. Sci. 427 (2018) 907–916.
[46] F. Yao, M. Jia, Q. Yang, F. Chen, Y. Zhong, S. Chen, L. He, Z. Pi, K. Hou, D. Wang, X. Li, Water Res. 193 (2021), 116881.
[47] Y. Wang, W. Zhou, R. Jia, Y. Yu, B. Zhang, Angew. Chem. Int. Ed. 59 (2020) 5350–5354.
[48] W.P. Utomo, H. Wu, Y.H. Ng, Small 18 (2022) 1–9.
[49] W.J. Foo, C. Zhang, G.W. Ho, Nanoscale 5 (2013) 759–764.
[50] L. Yuan, S.F. Hung, Z.R. Tang, H.M. Chen, Y. Xiong, Y.J. Xu, ACS Catal. 9 (2019) 4824–4833.
[51] B.R. Chen, V.H. Nguyen, J.C.S. Wu, R. Martin, K. Kočí, Phys. Chem. Chem. Phys. 18 (2016) 4942–4951.
[52] I. Knopf, C.C. Cummins, Organometallics 34 (2015) 1601–1603.
[53] Q. Zou, G. Long, T. Zhao, X. Hu, Green. Chem. 22 (2020) 1134–1138.
[54] M. Yousaf, M. Ahmad, Z.P. Zhao, J. CO_2 Util. 64 (2022), 102172.
[55] K.A. Grice, M.C. Groenenboom, J.D.A. Manuel, M.A. Sovereign, J.A. Keith, Fuel 150 (2015) 139–145.